Available online at www.sciencedirect.com
ScienceDirect
Trans. Nonferrous Met. Soc. China 34(2024) 2605−2618
Transactions of Nonferrous Metals Society of China
www.tnmsc.cn

Effect of wire diameter compression ratio on drawing deformation of micro copper wire

Tao HUANG[1], Han-jiang WU[1], Ke-xing SONG[1,2], Yan-min ZHANG[1], Yan-jun ZHOU[1], Shao-lin LI[1]

1. School of Materials Science and Engineering, Henan University of Science and Technology, Luoyang 471023, China;
2. Henan Key Laboratory of Advanced Conductor Materials, Institute of Materials, Henan Academy of Sciences, Zhengzhou 450000, China

Received 8 December 2023; accepted 28 June 2024

Abstract: A crystal plasticity finite element model was developed for the drawing deformation of pure copper micro wire, based on rate-dependent crystal plasticity theory. The impact of wire diameter compression ratio on the micro-mechanical deformation behavior during the wire drawing process was investigated. Results indicate that the internal deformation and slip of the drawn wire are unevenly distributed, forming distinct slip and non-slip zones. Additionally, horizontal strain concentration bands develop within the drawn wire. As the wire diameter compression ratio increases, the strength of the slip systems and the extent of slip zones inside the deformation zone also increase. However, the fluctuating stress state, induced by contact pressure and frictional stress, results in a rough and uneven wire surface and diminishes the stability of the drawing process.

Key words: micro copper wire; drawing deformation; crystal plasticity; finite element; slip mode

1 Introduction

Micro copper wire, known for its high strength and conductivity, is a vital component in signal transmission and is widely used in the electronic communication sector. There is a growing demand for micro wires with finer diameters and enhanced overall performance, driven by advancements in construction projects like 5G, big data, and the industrial internet, as well as progress in product integration and miniaturization [1−3]. The deformation process during drawing plays a crucial role in determining the performance of micro copper wires [4,5]. Previous macroscopic simulation studies often treated the wire as isotropic, overlooking the influence of the internal microstructure, such as grains and grain boundaries, on the drawing process. As wire diameters decrease to micron levels, the anisotropy of the crystal becomes more pronounced and cannot be ignored [6]. The conventional macroscopic models are inadequate for predicting the mechanical behavior of micro wires. Instead, microscopic simulations using crystal plasticity finite element analysis overcome these limitations by incorporating detailed structural characteristics.

In recent years, an increasing number of scholars have utilized the crystal plastic finite element method to investigate the effects of material microstructure on the plastic deformation of metal materials at the meso-scale [7]. LI et al [8] examined the impact of grain size and micro-structure on the shear properties of copper foil that is 100 μm-thick during the micro-blanking process. ZHANG et al [9] explored the compression process

Corresponding author: Han-jiang WU, Tel: +86-19562535917, E-mail: hanjiangwu@163.com;
Ke-xing SONG, Tel: +86-18838831461, E-mail: kxsong@haust.edu.cn
DOI: 10.1016/S1003-6326(24)66563-5

of Cu−Nb composites by employing the crystal plasticity finite element method, integrating the thermodynamics and kinetics principles. ARDELJAN et al [10] investigated the correlation between grain structures in annealed and cold deformation states, focusing on the phenomenon of strain localization during material compression. WANG et al [11] conducted an analysis of the effect of copper plate thickness on inhomogeneous deformation and shear strain evolution during material rolling deformation, observing that the surface grain of the copper plate exhibits greater slip resistance compared to the core grain. Additionally, WANG et al [12] explored the impact of geometric size and initial crystal orientation on texture evolution and the stress−strain response during material deformation using the crystal plasticity finite element method. LIANG et al [13] studied the effects of orientation and degree of deformation on the compression deformation process of materials, making predictions about the evolution of deformation microstructure and texture. MELLBIN et al [14] examined the impact of rolling temperature on the texture development of copper during hot rolling, revealing that the intensity of the rolling texture progressively increases with decreasing rolling temperatures. LATYPOV et al [15] analyzed the impact of initial texture on the microstructure and texture evolution of polycrystalline copper during multi-pass torsional extrusion. CHEN et al [16] studied the effect of grain size on the deformation process of copper foil rolling, noting that reducing the grain size enhances the activation of the initial slip system. ZHANG and DONG [17] discovered that the quantity of grains significantly influences the deformation inhomogeneity, shear band formation, and material strength in the micro-stretching process of copper foil.

Numerous scholars have conducted research on the deformation mechanism of copper foil during the rolling process using crystal plasticity finite element analysis. However, the microscopic deformation mechanisms of the micro copper wire in the drawing process remain unclear and need further investigation. Utilizing a crystal plasticity finite element model, we simulated and analyzed the anisotropic mechanical characteristics of the micro pure copper wire in the drawing process using Abaqus finite element software. We extensively investigated the effects of various wire diameter compression ratios on the drawing force, contact stress, metal flow law, non-uniform deformation, and slip system evolution during the drawing process of the micro pure copper wire. By studying the mechanical behavior of copper wire drawing under different wire diameter compression ratios, we aimed to gain a deeper understanding of the deformation characteristics during wire drawing. This understanding not only enables the prediction of potential risk areas such as cracks and fractures in the wire production but also facilitates the optimization of drawing process parameters to enhance the stability of fine copper wire production, reduce the rate of defective products, and lower production costs.

2 Model establishment and validation

2.1 Experimental materials

After six consecutive drawing deformations of pure copper wire with a diameter of 3 mm, a micro copper wire with a diameter of 180 μm was produced. Samples were taken from the longitudinal section of the wire for transmission electron microscopy (TEM) characterization. The obtained TEM samples underwent mechanical thinning and electrolytic double spraying. The microstructure of the samples was examined using an FEI Talos F200X electron microscope. Figure 1 displays the TEM image of the longitudinal section grains of the 180 μm-thick micro copper wire, showing significant elongation in the drawing direction. The grain shape inside the wire is primarily characterized by the elongated deformed

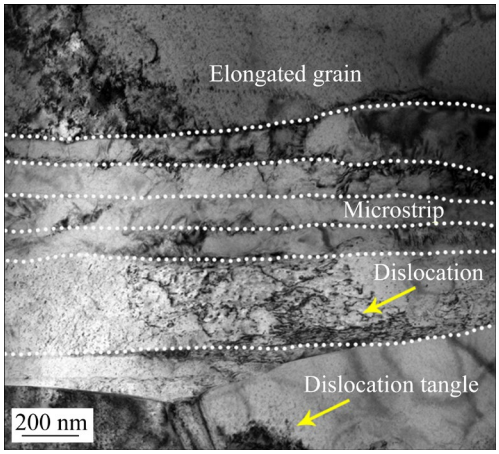

Fig. 1 TEM image of longitudinal grain structures in micro copper wire

grains. A significant quantity of dislocations is evident, with some becoming intertwined within the grains, resulting in the formation of high-density dislocations.

2.2 Crystal plasticity mechanics basis

The deformation rate during the elastic-plastic deformation of solids is characterized by the velocity gradient tensor ($\boldsymbol{L}$). This tensor is composed of the elastic velocity gradient tensor ($\boldsymbol{L}_e$) and the plastic velocity gradient tensor ($\boldsymbol{L}_p$) [18]:

$$\boldsymbol{L}=\boldsymbol{L}_e+\boldsymbol{L}_p \tag{1}$$

$\boldsymbol{L}_p$ is determined by dislocation slip [19], which satisfies:

$$\boldsymbol{L}_p=\sum_{\alpha=1}^{N}\dot{\gamma}^{\alpha}\boldsymbol{m}^{*\alpha}\otimes\boldsymbol{n}^{*\alpha} \tag{2}$$

where $\dot{\gamma}^{\alpha}$ is the slip shear strain rate on slip system α; $\boldsymbol{m}^{*\alpha}$ and $\boldsymbol{n}^{*\alpha}$ are the orthogonal non-unit vectors representing the slip direction and the normal direction of the slip surface after deformation of the slip system α, respectively; N denotes the number of slip systems.

The relationship between the shear strain rate $\dot{\gamma}^{\alpha}$ induced by dislocation motion within each slip system, the shear stress (τ^{α}) applied to the slip system and the critical shear stress (g^{α}) required for dislocation activation [20] are formulated into the following function:

$$\dot{\gamma}^{\alpha}=\dot{\gamma}_0^{\alpha}\left|\tau^{\alpha}/g^{\alpha}\right|^{1/m}\operatorname{sgn}(\tau^{\alpha}),\quad \tau^{\alpha}\geq\tau_c^{\alpha} \tag{3}$$

$$\dot{\gamma}^{\alpha}=0,\quad \tau^{\alpha}<\tau_c^{\alpha} \tag{4}$$

where $\dot{\gamma}_0^{\alpha}$ represents the reference shear strain rate for slip system α; τ_c^{α} is the critical resolved shear stress for slip system α; m indicates the strain rate sensitivity coefficient of slip system α. When m=0, the material behaves as a viscoelastic material. When $m\rightarrow 0$, the material behaves as a rate-independent one. When $\tau^{\alpha}\geq\tau_c^{\alpha}$, the slip system α initiates, leading to plastic deformation. Conversely, it is commonly assumed that the shear strain rate is zero, rendering the slip system inactive, and resulting in the absence of plastic deformation behavior.

The expression for the critical decomposition shear stress rate ($\dot{g}^{\alpha}$) is given as follows:

$$\dot{g}^{\alpha}=\sum_{\beta=1}^{N}h_{\alpha\beta}\left|\dot{\gamma}^{\beta}\right| \tag{5}$$

where $h_{\alpha\beta}$ is the slip system hardening coefficient.

The slip system hardening coefficient $h_{\alpha\beta}$ is divided into the self-hardening coefficient $h_{\alpha\alpha}$ ($\alpha=\beta$) and the latent hardening coefficient $h_{\alpha\beta}$ ($\alpha\neq\beta$). Typically, the ratio between the latent hardening coefficient and the self-hardening coefficient (q) ranges from 1.0 to 1.5, and their relationship satisfies the following equation [21,22]:

$$h_{\alpha\beta}=qh_{\alpha\alpha}\quad(\alpha\neq\beta) \tag{6}$$

$$h_{\alpha\alpha}=h(\gamma)=h_0\operatorname{sech}^2\left|\frac{h_0\gamma}{\tau_s-\tau_0}\right| \tag{7}$$

where h_0 represents the initial hardening modulus; τ_s denotes the saturation value of the critical shear stress; τ_0 indicates the critical value of the initial shear stress; γ expresses the cumulative shear strain of all slip systems, which satisfies:

$$\gamma=\sum_{\alpha=1}^{N}\int_0^t\left|\dot{\gamma}^{\alpha}\right|\mathrm{d}t \tag{8}$$

where t is the time.

2.3 Key technology of model establishment

2.3.1 Acquisition of key mechanical parameters

The pure copper micro wire analyzed in this study is a metallic material with a face-centered cubic crystal structure. The plastic deformation process in pure copper involves dislocation slip, occurring across 12 slip systems of {111}⟨110⟩, as detailed in Table 1 [23]. To simulate the drawing and forming processes of micro copper wire using crystal plasticity finite elements, it is crucial to ascertain the parameters of the material's constitutive model accurately. In this study, the wire was elongated using a tensile testing machine (Fig. 2). The crystal plasticity finite element method was then applied to modeling the stretching process of the micro copper wire. By adjusting the plastic parameters for each crystal, the stress−strain curves were aligned from wire tensile simulations with experimental results to ensure maximum consistency. Figure 2 illustrates the stress−strain curves from both the simulation and experiment, showing a high level of agreement. The material constitutive model was established based on these determined parameters, and the constitutive model parameters for the micro copper wire are presented in Table 2. A detailed interpretation and inter-relation of each parameter in the constitutive model are discussed in Section 2.2, focusing on the fundamentals of crystal plasticity mechanics.

Table 1 Slip systems of pure copper material in this study [23]

Slip system	Slip plane	Slip direction	Slip system	Slip plane	Slip direction
$a1$		$[0\bar{1}1]$	$b1$		[101]
$a2$	(111)	$[10\bar{1}]$	$b2$	$(\bar{1}11)$	[110]
$a3$		$[\bar{1}10]$	$b3$		$[0\bar{1}1]$
$c1$		[011]	$d1$		[011]
$c2$	$(1\bar{1}1)$	[110]	$d2$	$(11\bar{1})$	[101]
$c3$		$[10\bar{1}]$	$d3$		$[\bar{1}10]$

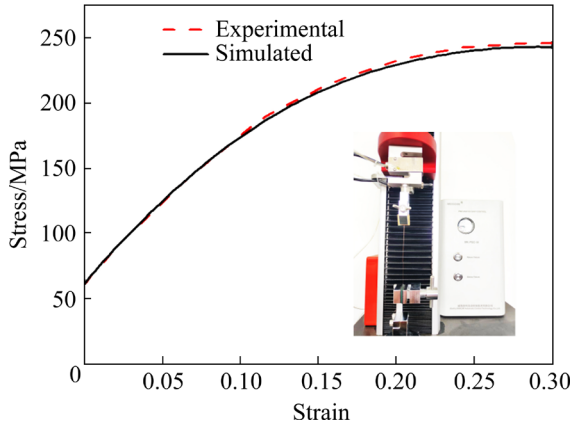

Fig. 2 Tensile testing machine and comparison of stress−strain curves of micro copper wire obtained by experiment and crystal plasticity finite element simulation

Table 2 Constitutive model parameters of pure copper

C_{11}/ GPa	C_{12}/ GPa	C_{44}/ GPa	N	$\dot{\gamma}_0$/ s^{-1}	h_0/ MPa	τ_s/ MPa	τ_0/ MPa	q
168.4	121.4	75.4	10	0.001	90	54	12	1.0

C_{11}, C_{12} and C_{44} are elastic moduli of pure copper

2.3.2 Determination of deformation characteristics

The micro wire drawing model proposed in this study assumes plane strain [24]. The drawing direction is designated as the X-axis, the normal direction as the Y-axis, and the transverse direction as the Z-axis. Figure 3 provides a schematic of the wire drawing deformation and the corresponding coordinate system.

2.3.3 Convergence calculation

In industrial production, the wire drawing process involves deforming micron-scale materials at high strain rates. Achieving convergence in the results of the crystal plasticity model under these conditions is challenging due to the effects of high strain rates and small scale. Addressing this issue requires iterative adjustments to the incremental step size and the contact conditions between the drawing die and the wire. Additionally, setting the output frequency of field variables to match the increment step size enables efficient computation of high-speed material deformation processes.

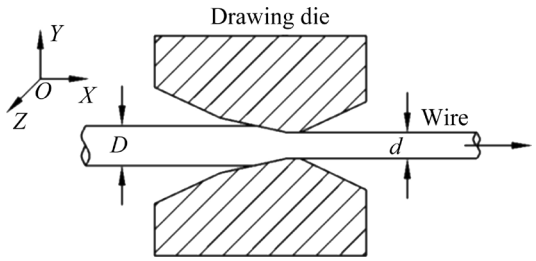

Fig. 3 Schematic diagram of micro wire drawing

2.3.4 Deformation body setting and meshing

During the pre-processing stage of setting up the crystal plasticity finite element model to simulate the drawing deformation of a micro copper wire, the micro copper wire is designated as the deformable body, the drawing die is defined as the rigid body, and the micro wire model is discretized using CPE4R elements.

2.3.5 Key process parameters setting

Producing microfine copper wire involves regulating the drawing process by setting the wire drawing speed and controlling the friction between the drawing die and the wire. Research indicates that the friction coefficient between the drawing die and the copper wire typically ranges from 0.03 to 0.11 [25]. In crystal plasticity finite element model of this study, the drawing speed is set to be 1 m/s, and the friction coefficient between the drawing die and the wire is fixed to be 0.07.

200 representative grain orientations were extracted from the EBSD experimental data to serve as the initial grain orientation for the model. Based on the grain shape and orientation data acquired from the experiment, the crystal plasticity finite element model of the micro copper wire with a diameter of 180 μm is ultimately developed (Fig. 4).

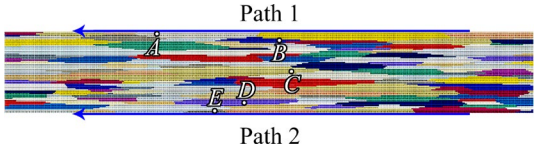

Fig. 4 Crystal plasticity finite element model of micro copper wire

2.4 Model validation

In practical scenarios, it is not possible to directly observe different crystallographic directions or crystal planes in samples. Instead, one can only discern the morphology of grains. To establish a relationship between the internal grain structure of the material and its macroscopic deformation, it is crucial to understand how grain orientation varies within the deformed material. Material processing operations such as rolling and stretching introduce stress fields that significantly alter the grain orientation, impacting mechanical properties of the materials. Pole figures are utilized to observe material deformation behavior at the microscopic level, revealing the primary orientation distribution of grains in the material. If the crystal plasticity finite element model developed can accurately predict grain orientation, this confirms its reliability in describing the grain structure and deformation behavior [26].

The simulation of the drawing process, which reduces the diameter of micro pure copper wire from 320 to 180 μm, was conducted using the calibrated crystal plasticity parameters. The drawing speed was set to be 1 m/s, and the friction coefficient was established to be 0.07. The comparison of simulated and experimental {100} pole figures are displayed in Fig. 5. This figure highlights the emergence of a fiber texture within the wire following drawing, indicating a specific level of deformation. The presence of a ⟨100⟩ texture inside the wire post-drawing suggests that the ⟨100⟩ crystal orientation of most grains within the wire has aligned with the drawing direction. The pole diagram derived from the crystal plasticity finite element simulation closely matches the pole figure obtained from electron backscattered diffraction (EBSD) experiments, thereby verifying the credibility of the developed crystal plasticity finite element model.

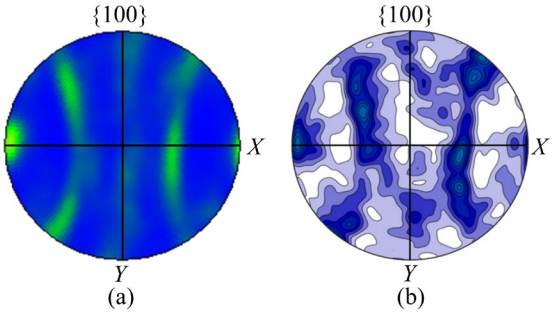

Fig. 5 Comparison of experimental (a) and simulated (b) {100} pole figures

3 Results and discussion

3.1 Stress and strain

Figure 6 illustrates the distribution of von Mises stress within the drawn wire at various compression ratios of wire diameter. As the drawing process progresses, a significant stress gradient is observed along the radial direction, both within the drawing deformation zone of the wire and inside the drawn wire. A high-stress zone is observed in the surface layer within the drawing deformation zone, depicted by the red zone. Additionally, a medium-stress zone is present in the surface layer, also shown in the green zone, while a low-stress zone is evident in the core part of the drawn wire, represented by the blue zone. As the wire diameter compression ratio increases, the von Mises stress value within the wire also increases. The high-stress region and the medium-stress region within the wire progressively extend from the surface towards the core, while the low-stress area in the core diminishes in size.

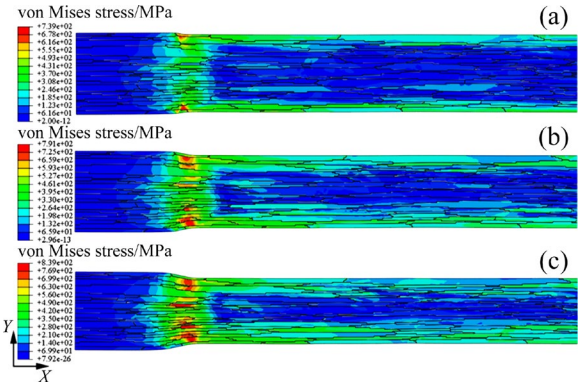

Fig. 6 von Mises stress distribution in wire models at different wire diameter compression ratios: (a) 10%; (b) 20%; (c) 30%

Figure 7 illustrates the correlation between the stress at internal marked points of the drawn wire and the drawing time, with a wire diameter compression ratio of 20%. Points *A*, *B*, *C*, *D*, and *E* are located on different sections of the wire (as shown in Fig. 4), specifically on the upper surface, upper surface layer, core, lower surface layer, and lower surface, respectively. The diagram reveals that the three-dimensional stress state within the

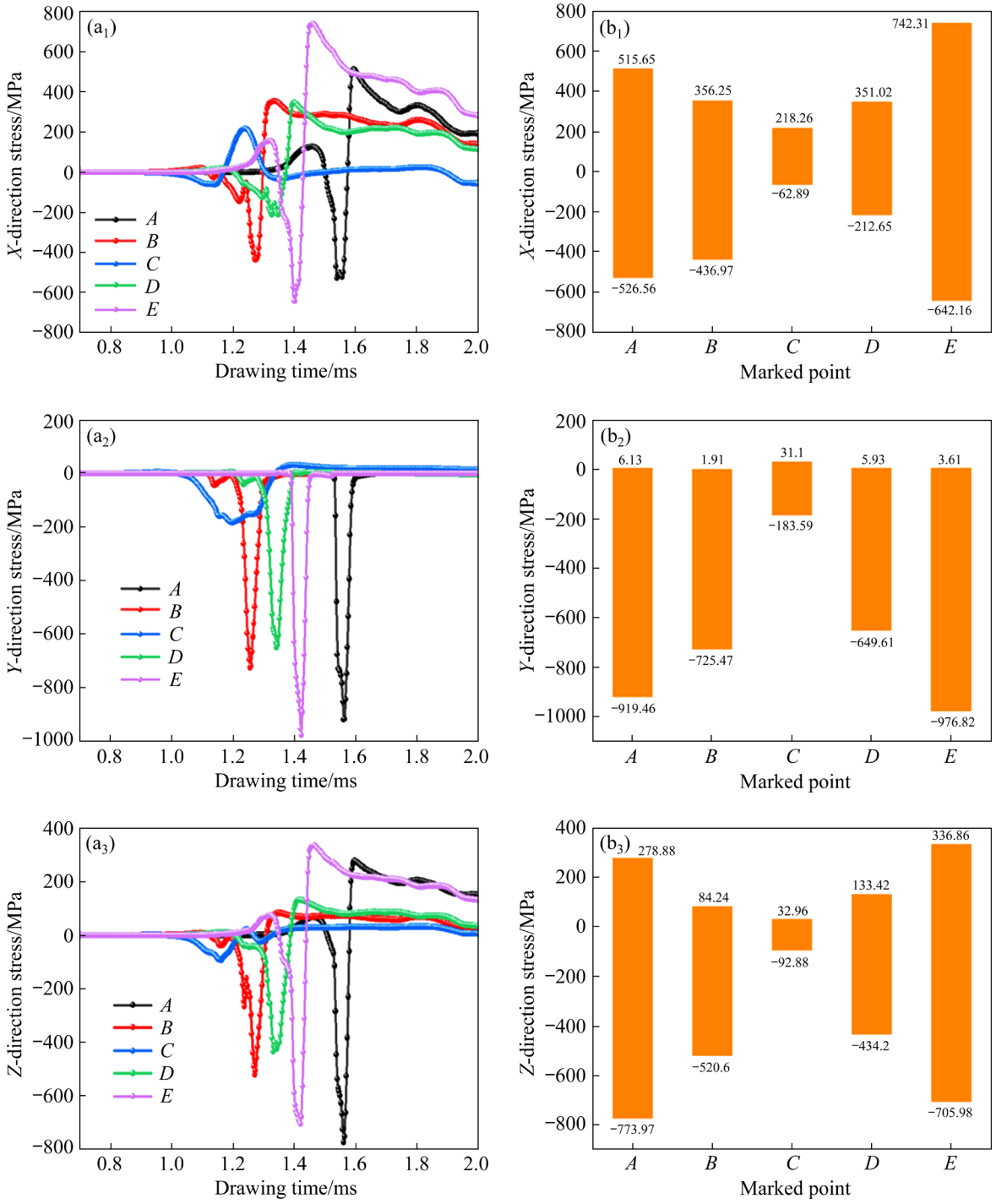

Fig. 7 Stress variation in relation to drawing time at internal marked points in Fig. 4 within drawn wire: (a_1–a_3) Stress–time curves of marked points; (b_1–b_3) Stress limit of marked points

wire varies significantly at different positions in response to changes in drawing time. Notably, the stress in the *X* and *Z* directions on the longitudinal section of the wire exhibits pronounced fluctuation during the drawing process, characterized by distinct alternating positive and negative variations. This dynamic arises due to changes in the stress field surrounding a point as a result of ongoing deformation. The stress at any specific point within the wire gradually increases and decreases as the deformation is applied and removed, respectively. Moreover, the stress values at each point within the wire display a consistent pattern from the highest to the lowest, moving from the surface to the surface layer, and then to the core, consistent with the stress distribution depicted in Fig. 6.

Figure 8 shows the distribution of maximum principal plane strain during the wire drawing process at different wire diameter compression ratios. The diagram highlights a strain concentration zone evident in the horizontal direction within the depicted wire. The distribution of this strain concentration zone is non-uniform within the wire. At a wire diameter compression ratio of 10%, the strain concentration zone is primarily localized near the surface of the wire. As the wire diameter compression ratio increases, there is a significant rise not only in the number of strain concentration zones within the wire but also in the continuously escalating maximum principal plane strain value. At the micro level, an increase in wire diameter compression ratio intensifies the internal wire deformation.

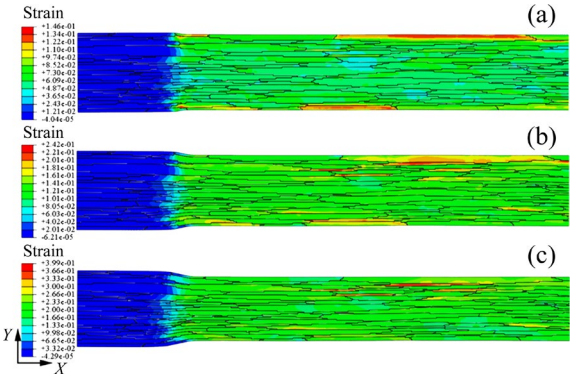

Fig. 8 Maximum principal plane strain distribution during wire drawing process at different wire diameter compression ratios: (a) 10%; (b) 20%; (c) 30%

Figure 9 presents the correlation between the strain at internal marked points (Fig. 4) of the drawn wire and drawing time at a wire diameter compression ratio of 20%. This figure shows that the strain in the X and Y directions is distributed nearly symmetrically. Data extraction reveals that the strain in the Z direction is zero, indicating that the deformation zone of the drawn wire is in a plane strain state. Additionally, during the initial stage of deformation in the drawing process, the strain in the

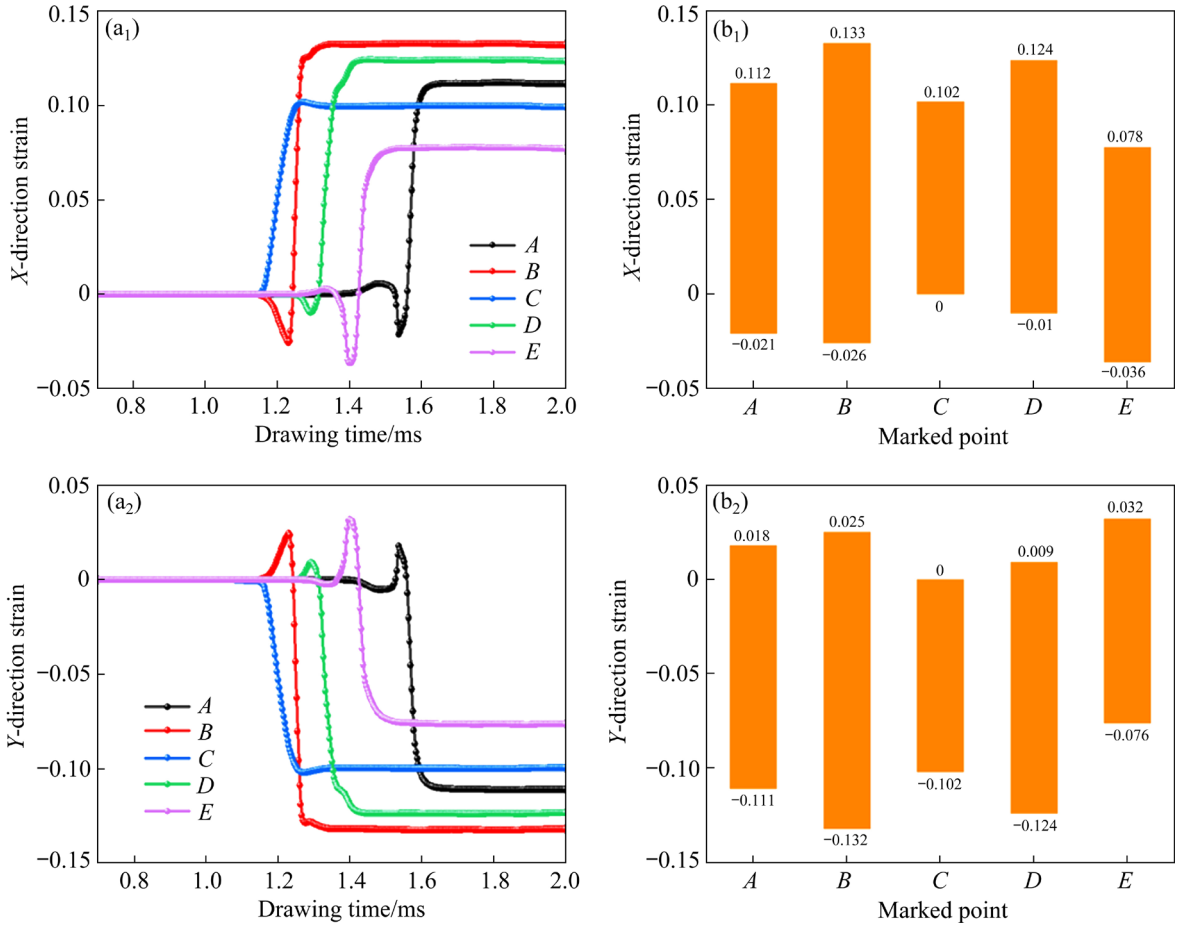

Fig. 9 Strain variation in relation to drawing time at marked points in Fig. 4 within drawn wire: (a_1, a_2) Strain−time curve of marked points; (b_1, b_2) Strain limit of marked points

surface and surface layer of the drawn wire exhibits alternating positive and negative directions. Notably, prior to the onset of deformation, the strain value remains at zero. When the drawing die aligns with the wire surface at each point in the vertical direction, the strain value at that specific point reaches its peak. Subsequently, the maximum strain value at that position remains constant during the later stage of deformation. Furthermore, the strain values vary at different positions within the wire: the strain at the core position is smaller than that in the surface and surface layer, and the strain in the surface layer is larger than that at other four positions. This variability is due to the non-uniform deformation resulting from variations in the microstructure of grains located at different positions within the wire.

3.2 Contact stress and metal flow

Figure 10 illustrates the calculated contact pressure and friction stress in the drawing deformation zone of a micro copper wire model at

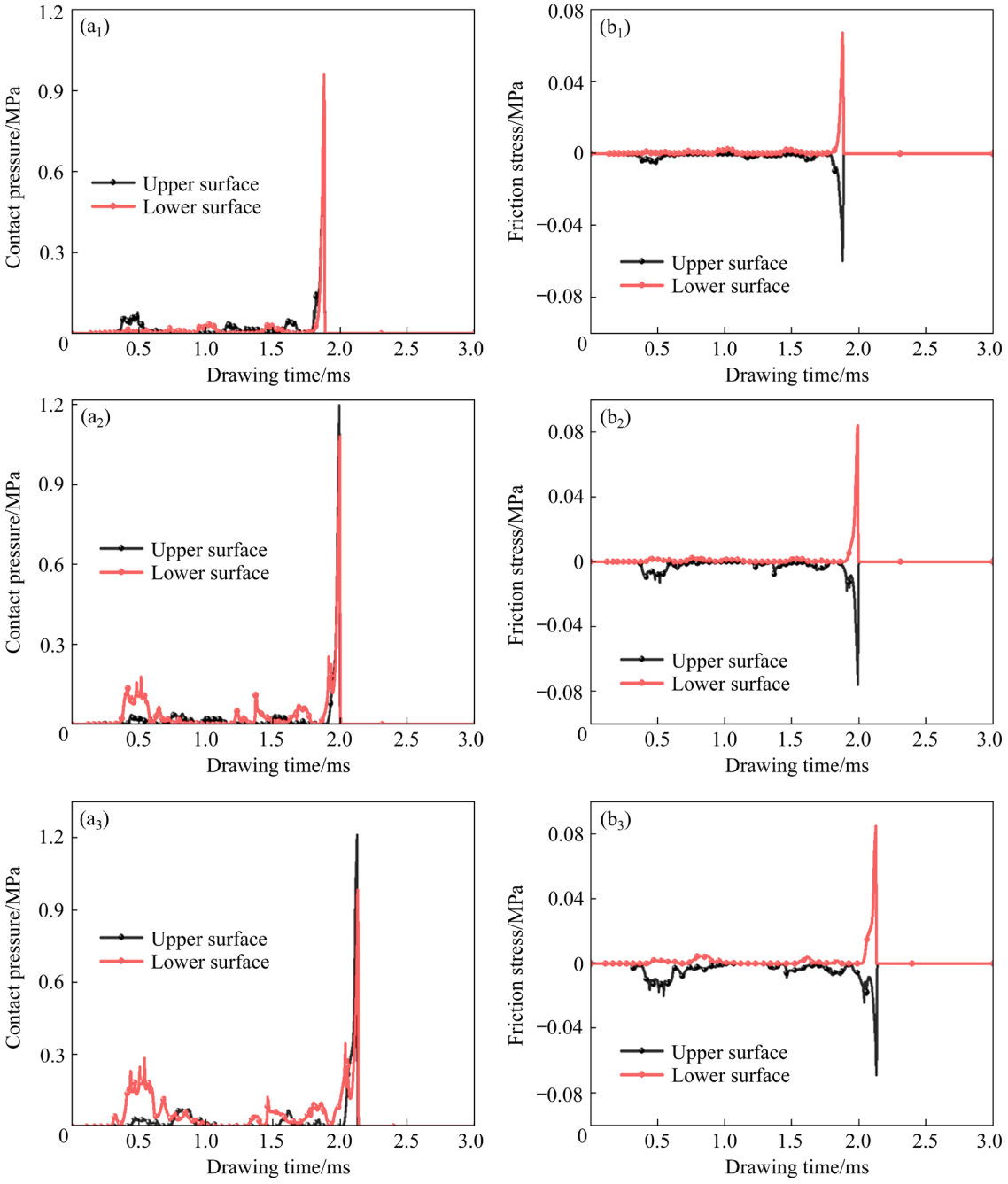

Fig. 10 Contact pressure and friction stress in drawing deformation zone for wire models at different wire diameter compression ratios of 10% (a_1, b_1), 20% (a_2, b_2) and 30% (a_3, b_3): (a_1−a_3) Contact pressure−time curves; (b_1−b_3) Friction stress−time curves

three wire diameter compression rates of 10%, 20%, and 30%. The figure features black and red curves representing the variations in contact pressure and friction stress on the upper and lower surfaces of the wire as they interact with the drawing die over time. The terms “contact pressure” and “friction stress” are often collectively referred to as “contact stress” [27−29].

Figure 10 shows that the contact pressure curves and the friction stress curves on the upper and lower surfaces of the wire are oriented in the same and opposite directions, respectively. There are noticeable differences between the contact stress state curves of the upper and lower surfaces. These variations are attributed to the differences in grain orientation, shape, and boundary positions on the upper and lower surfaces in contact with the drawing die. The fluctuation in contact pressure and friction stress during the wire drawing process is influenced by various factors, which exacerbate the deformation and stress distribution on the wire surface. After the completion of the drawing process, the wire surface is rough and uneven. As the wire diameter compression ratio of increases, the extent of drawing deformation grows, extending progressively into the inner regions of the wire and leading to increased resistance to deformation during the wire plastic deformation of the wire. This results in elevated levels of contact pressure and friction stress. Additionally, the contact pressure on the surface of the wire is higher as the wire enters and exits the drawing die compared to that experienced during the drawing process. Upon exiting the drawing die, the contact pressure and friction stress reach their maximum levels given the wire current diameter condition.

Figure 11 displays the displacement variations along the upper and lower surfaces of drawn wire models subjected to different wire diameter compression rates. Here, $U1$ and $U2$ denote the axial and radial displacements of the wire, respectively. The head of the wire is in contact with the drawing die, while the tail is positioned away from the die. Displacement is a crucial parameter reflecting the metal flow behavior during metal plastic deformation processes [30]. To analyze the

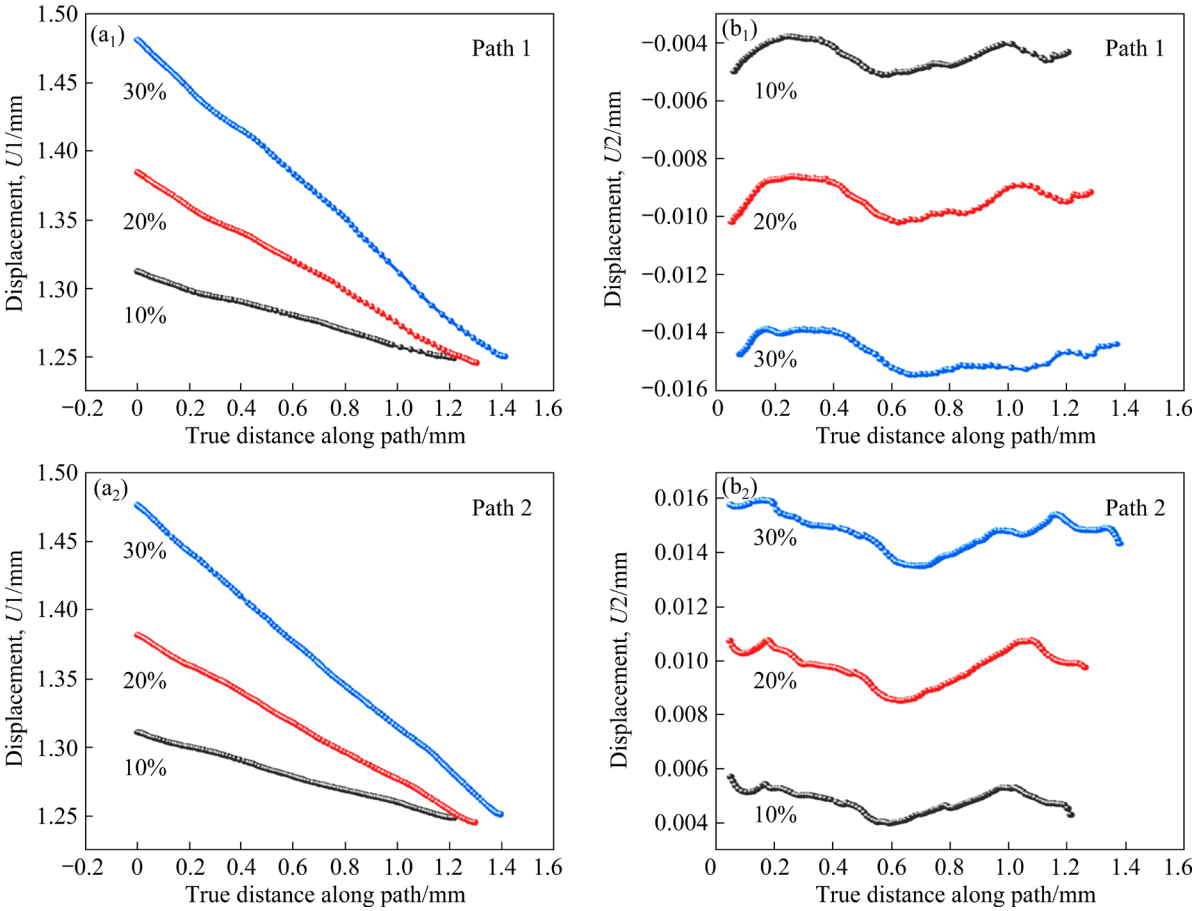

Fig. 11 Displacement variation in wire model with different wire diameter compression ratios along Paths 1 and 2 in Fig. 4

metal flow pattern on the wire surface during the drawing process, displacement field information was extracted along Path 1 and Path 2. These paths represent selected horizontal trajectories along the upper and lower surfaces of the wire, as indicated in Fig. 4.

Figure 11 reveals that the axial displacement of both the upper and lower surfaces of the wire remains relatively constant, decreasing gradually from the head to the tail of the wire. Positive axial displacement indicates that the metal flows in the drawing direction, resulting in the elongation of the wire in that direction. The elongation varies between the upper and lower surfaces, potentially leading to a non-flat end face of the drawn wire. Furthermore, the radial displacement directions on the upper and lower surfaces are opposite, indicative of bidirectional metal flow. The radial displacement values are unequal and non-linear, reflecting the actual roughness of the wire surface. This disparity is attributed to variations in grain orientations of the wire, leading to differential ease of slip deformation and varying displacement magnitudes. As the wire diameter compression ratio increases, both axial and radial displacements on the upper and lower surfaces increase. This escalation, driven by the heightened wire deformation due to increased compression, enhances the metal flow, consequently leading to an increase in displacement values under consistent working conditions.

3.3 Slip system

During the wire drawing process, the macroscopic effect of work-hardening significantly enhances the mechanical properties of the material. On a microscopic level, this is reflected by an increase in deformation resistance within the material [31]. Figure 12 illustrates the strength of the slip system associated with three different wire diameter compression ratios following the drawing deformation. In this figure, “SDV3” represents the strength of the primary slip system, labeled a3, which is one of the 12 slip systems present in pure copper. The strength of a slip system relates to its ability to resist deformation caused by slip movements within the material (microscopic deformation mechanisms in metal materials). The magnitude of this deformation resistance plays a crucial role in determining both the challenge and intensity of slip deformation. The greater the deformation resistance is, the more significant the material deformation is, thereby increasing the difficulty of the deformation process.

Figure 12 depicts an uneven distribution of strength in the slip system at various positions of the drawn wire, indicating a gradient distribution. The strength of the slip system decreases continuously from the surface to the core of the wire. During plastic deformation, slip typically initiates on the free surface of the grain and moves towards the interior. It then encounters a blockage at the grain boundary, leading to the formation of a deformation resistance concentration zone, which is depicted in the red area of the figure. At a wire diameter compression rate of 10%, this concentration zone of deformation resistance is primarily located in the surface layer of the wire, resulting in relatively low strength of the slip system. As the deformation level increases, the deformation resistance zone in the wire progressively extends from the surface layer toward the core. When the compression rate of the wire diameter reaches 30%, nearly all the grains in the wire after drawing show significant deformation resistance. At this stage, there is an increase in the potency of the slip system, leading to heightened material deformation.

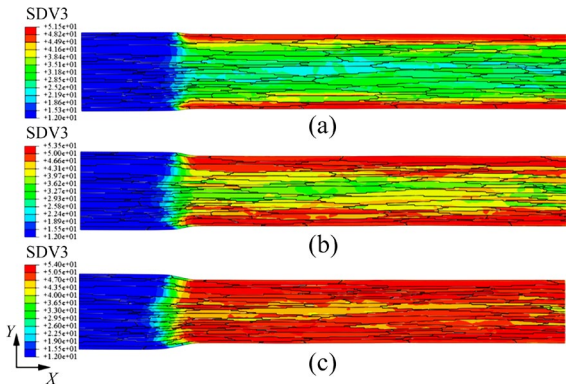

Fig. 12 Strength of wire slip system at different wire diameter compression ratios: (a) 10%; (b) 20%; (c) 30%

Figure 13 illustrates the changes in slip system strength of marked points (Fig. 4) in the wire during the drawing process with a wire diameter compression ratio of 20%. The diagram shows that deformation within the drawn wire varies at different positions, leading to unevenness, and the strength values of the slip systems differ at different

positions. The slip system strength in the wire surface and the surface layer, relative to the core position, exhibits higher value. The presence of a strain concentration zone in the wire surface layer may lead to the maximum slip system strength value. This observation is consistent with the distribution of slip system strength in the drawn wire as illustrated in Fig. 12.

Figure 14 illustrates the slip evolution in a specific slip system in the wire drawing process at three different wire diameter compression ratios. “SDV153” denotes the slip activation zone of the a3 slip system. In the diagram, the red zone within the wire is assigned a value of 1, indicating activated slip, while the blue zone has a value of 0, signifying no slip activation. The diagram reveals that due to variations in orientation and grain shape between neighboring grains, different grains deform unequally under the same deformation conditions. This results in an uneven distribution of slip zones in the wire post-drawing deformation, distinguishing between areas of slip and no slip. Slip typically initiates on the surfaces of grains and at grain boundaries. As the drawing time progresses, the slip propagates horizontally against the drawing direction towards the grain interior, eventually covering the entire grain thickness.

Throughout the wire drawing process, the distribution of slip zones varies significantly across different grains. The position of the wire and the size of the grains vary markedly. Some grains are completely covered by the slip zone, while for others, the slip zones only cover specific local areas within the grains, leading to localized slip

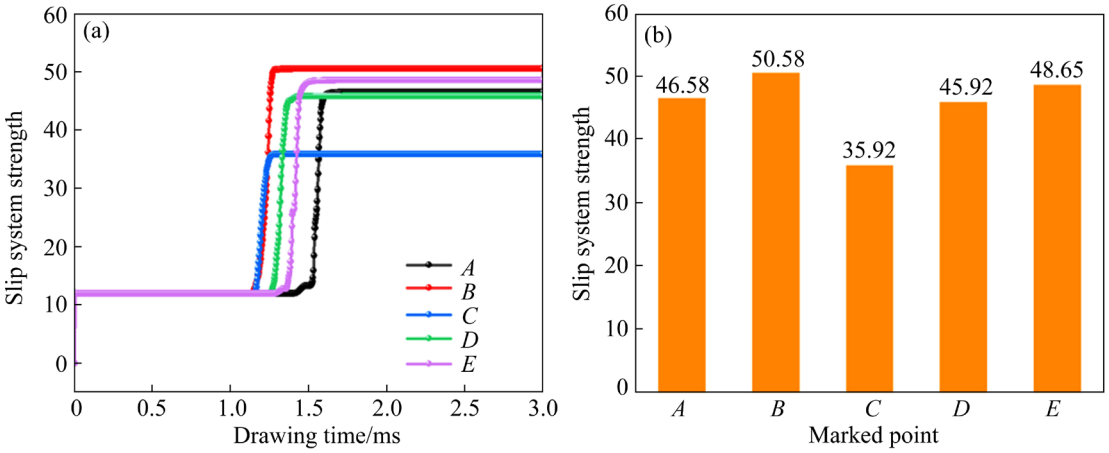

Fig. 13 Slip system strength variation of marked points in Fig. 4 in wire in relation to drawing time: (a) Slip system strength−time curve of marked points; (b) Slip system strength limit of marked points

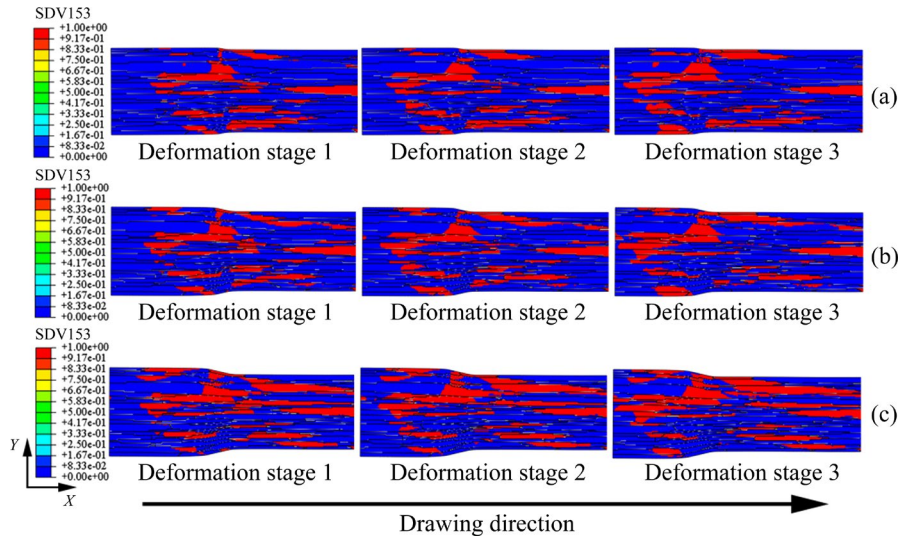

Fig. 14 Slip evolution in wire drawing deformation zone at different wire diameter compression ratios: (a) 10%; (b) 20%; (c) 30%

deformation. As the wire diameter compression rate increases, the slip zone in the wire also expands. Consequently, the augmented sliding area primarily concentrates in the wire surface layer. When the compression ratio of the wire diameter reaches 30%, not only does the surface layer of the wire increase, but also the sliding area in the core of the wire expands. This indicates that as deformation reaches a certain threshold, the drawing deformation of the wire gradually extends from the surface to the core. This microscopic perspective elucidates that enhancing the compression rate of the wire diameter can improve metal flow and extend plastic deformation in the drawn wire.

4 Conclusions

(1) When the wire undergoes minimal deformation, stress concentration and strain concentration primarily occur on the wire surface. However, as the wire diameter compression ratio increases, slip deformation progressively moves towards the core of the wire, resulting in elevated internal stress and strain.

(2) An increase in the wire diameter compression ratio slightly raises the contact pressure and friction stress in the deformation zone of the wire drawing, potentially reducing the surface integrity and smoothness of the process.

(3) With an increase in the wire diameter compression ratio, both axial and radial displacement values on the upper and lower surfaces of the wire rise, indicating more vigorous metal flow.

(4) The strength and distribution of slip systems vary at different positions of the drawn wire. There is a gradual reduction in the strength of slip systems from the wire surface to the core, leading to a division of the wire into regions with and without slip activity.

CRediT authorship contribution statement

Tao HUANG: Conceptualization, Project administration, Funding acquisition; **Han-jiang WU:** Writing − Original draft, Investigation, Data curation; **Ke-xing SONG:** Writing − Review & editing, Software, Validation, Formal analysis; **Yan-min ZHANG:** Visualization, Supervision, Software, Resources; **Yan-jun ZHOU:** Methodology, Software, Investigation; **Shao-lin LI**: Visualization, Data curation.

Declaration of competing interest

The authors declare that they have no known competing financial interests or personal relationships that could have appeared to influence the work reported in this paper.

Acknowledgments

This work was supported by the National Natural Science Foundation of China (Nos. U21A2051, 52173297, 52071133), the R&D Projects of Henan Academy of Sciences of China (No. 220910009), the Key R & D and Promotion Projects of Henan Province of China (No. 212102210441), the Joint Fund of Henan Science and Technology R&D Plan of China (No. 222103810037), and the Zhongyuan Scholar Workstation Funded Project of China (No. 214400510028).

References

[1] ZHANG Peng-fei, ZHOU Yan-jun, LIU Ya-hui, LI Shao-lin, SONG Ke-xing, CAO Jun, WU Bao-an, LI Xin, WU Han-jiang, GU Ji-hua. Strengthening mechanism of ultra-high strength Cu−20Ag alloy wire induced by cumulative strain [J]. Materials Science and Engineering A, 2022, 855: 1−11.

[2] CHENG Chu, SONG Ke-xing, MI Xu-jun, WU Bao-an, XIAO Zhu, XIE Hao-feng, ZHOU Yan-jun, GUO Xiu-hua, LIU Hai-tao, CHEN Ding-biao, SHEN Xiao-yu, DING Yong. Microstructural evolution and properties of Cu−20wt.%Ag alloy wire by multi-pass continuous drawing [J]. Nanotechnology Reviews, 2020, 9: 1359−1367.

[3] SONG Ke-xing, GENG Yong-feng, BAN Yi-jie, ZHANG Yi, LI Zhou, MI Xu-Jun, CAO Jun, ZHOU Yan-jun, ZHANG Xu-bin. Effects of strain rates on dynamic deformation behavior of Cu−20Ag alloy [J]. Journal of Materials Science and Technology, 2021, 79: 75−87.

[4] AMIRHOSSEIN J, HAMED J A, MOHAMMAD R, ROOHOLLAH J. Effect of extrusion speed on properties of Cu−5vol.%Ti_2SnC composite wire fabricated by friction stir back extrusion process [J]. Transactions of Nonferrous Metals Society of China, 2024, 34: 935−951.

[5] LIU Ru-xue, LI Kai, ZHOU Guo-wei, TANG Wei-qin, SHEN Yao, TANG Ding, LI Da-yong. Simulation of strain induced abnormal grain growth in aluminum alloy by coupling crystal plasticity and phase field methods [J]. Transactions of Nonferrous Metals Society of China, 2022, 32: 3873−3886.

[6] JIANG Zhi-wei, YIN Dong-di, WAN You-fu, NI Ran, ZHOU Hao, ZHENG Jiang, WANG Qu-dong. Operating slip modes and inhomogeneous plastic deformation of Mg−10Gd−3Y−0.5Zr alloy during compression [J]. Transactions of Nonferrous Metals Society of China, 2023, 33: 79−94.

[7] DODLA S, BERTRAM A, KRÜGER M. Finite element

simulation of lamellar copper-silver composites [J]. Computational Materials Science, 2015, 101: 29−38.

[8] LI Xiao, LI Xiu-cheng, MISRA R D K, CHEN Zhang-hua. Grain size effect on shearing performance of copper foil: A polycrystal plasticity investigation [J]. Mechanics of Materials, 2022, 166: 1−12.

[9] ZHANG Y B, SONG S J, LIU F. Thermo-kinetic orientation study on interface behavior of polycrystalline Cu−Nb composite by crystal plasticity finite element method [J]. Materials & Design, 2022, 223: 1−12.

[10] ARDELJAN M, KNEZEVIC M, NIZOLEK T, BEYERLEIN I J, MARA N A, POLLOCK T M. A study of microstructure-driven strain localizations in two-phase polycrystalline HCP/BCC composites using a multi-scale model [J]. International Journal of Plasticity, 2015, 74: 35−57.

[11] WANG Rui, LU Cheng, LI Jia-qing, ZHANG Che, YU Hai-liang, MICHAL G. Microstructural evolution in pure copper during accumulative skin pass rolling: Experimental and crystal plasticity numerical investigations [J]. Journal of Materials Research and Technology, 2021, 14: 1903−1913.

[12] WANG Cheng, WANG Xiao-gui, WANG Chuan-li, WU Guang, LAI Yong-bin. A comparative study of plastic deformation behaviors of OFHC copper based on crystal plasticity models in conjunction with phenomenological and dislocation density-based hardening laws [J]. Journal of Materials Science, 2021, 56: 8789−8814.

[13] LIANG Yu-long, JIANG Shu-yong, ZHANG Yan-qiu, ZHAO Ya-nan, SUN Dong, ZHAO Cheng-zhi. Deformation heterogeneity and texture evolution of NiTiFe shape memory alloy under uniaxial compression based on crystal plasticity finite element method [J]. Journal of Materials Engineering and Performance, 2016, 26: 2671−2682.

[14] MELLBIN Y, HALLBERG H, RISTINMAA M. Recrystallization and texture evolution during hot rolling of copper,studied by a multiscale model combining crystal plasticity and vertex models [J]. Modelling and Simulation in Materials Science and Engineering, 2016, 24: 1−20.

[15] LATYPOV M I, LEE M G, BEYGELZIMER Y, PRILEPO D, GUSAR Y, KIM H S. Modeling and characterization of texture evolution in twist extrusion [J]. Metallurgical and Materials Transactions A, 2016, 47: 1248−1260.

[16] CHEN Shou-dong, LIU Xiang-hua, LIU Li-zhong. Effects of grain size and heterogeneity on the mechanical behavior of foil rolling [J]. International Journal of Mechanical Sciences, 2015, 100: 226−236.

[17] ZHANG Hai-ming, DONG Xiang-huai. Experimental and numerical studies of coupling size effects on material behaviors of polycrystalline metallic foils in microscale plastic deformation [J]. Materials Science and Engineering A, 2016, 658: 450−462.

[18] CHEN Shou-dong, LIU Xiang-hua, LIU Li-zhong. Grain statistics effect on deformation behavior in asymmetric rolling of pure copper foil by crystal plasticity finite element model [J]. Transactions of Nonferrous Metals Society of China, 2015, 25: 3370−3380.

[19] ASARO R J, NEEDLEMAN A. Overview No. 42 texture development and strain hardening in rate dependent polycrystals [J]. Acta Metallurgica Sinica (English Letters), 1985, 33: 923−953.

[20] PEIRCE D, ASARO R J, NEEDLEMAN A. Material rate dependence and localized deformation in crystalline solids [J]. Acta Metallurgica Sinica (English Letters), 1983, 31: 1951−1976.

[21] HU Li, JIANG Shu-yong, SHI Lai-xin, ZHANG Yan-qiu. Prediction of grain scale plasticity of NiTi shape memory alloy based on crystal plasticity finite element method [J]. Transactions of Nonferrous Metals Society of China, 2019, 29: 775−784.

[22] LI Kai-di, HAN Xiao-ning, TANG Bin, ZHANG Meng-qi, LI Jin-shan. Effect of microvoids on microplasticity behavior of dual-phase titanium alloy under high cyclic loading (I): Crystal plasticity analysis [J]. Transactions of Nonferrous Metals Society of China, 2022, 32: 513−523.

[23] CHEN Shou-dong, LIU Xiang-hua, LIU Li-zhong. Symmetric and asymmetric rolling pure copper foil: Crystal plasticity finite element simulation and experiments [J]. Acta Metallurgica Sinica (English Letters), 2015, 28: 1024−1033.

[24] CHEN Shou-dong, LIU Xiang-hua, LIU Li-zhong. Size effect mechanism on foil rolling analyzed by crystal plasticity finite element method [J]. Advanced Materials Research, 2015, 1424: 1424−1428.

[25] NARAYANAN K R, SRIDHAR I, SUBBIAH S. Experimental and numerical investigations of the texture evolution in copper wire drawing [J]. Applied Physics A, 2012, 107: 485−495.

[26] FAN Wan-wan, REN Zhong-kai, HOU Jie. Finite element simulation of mesoscale inhomogeneous deformation in 304 stainless steel foil tensile [J]. Materials Research Express, 2019, 6: 1−11.

[27] LIUDMIA V R, DMITRY V G, ROMAN A L, IVAN N E. Experimental determination and calculation of the wire drawing force in monolithic dies on straight-line drawing machines [J]. Machines, 2023, 11: 252.

[28] MUHAMMAD N, TULAYA D, DESMOND Y R C, SURAPONG C. Effects of custom-made insole materials on frictional stress and contact pressure in diabetic foot with neuropathy: Results from a finite element analysis [J]. Applied Sciences, 2021, 11: 1−11.

[29] LI Qian-kun, YAN Hong, CHEN Rong-shi. Effect of rolling reduction on deformation mechanism and twinning behavior of WE43 magnesium alloy [J]. Transactions of Nonferrous Metals Society of China, 2022, 32: 3901−3913.

[30] ZHANG Yu-heng, HU Zhi-qing, GUO Li-ming. Study on a new forming method—Thread rolling by crystal plasticity finite element simulation [J]. Metals, 2021, 11: 1−16.

[31] LI Zi-han, ZHOU Guo-wei, LI Da-yong, WANG Hua-miao, TANG Wei-qin, PENG Ying-hong, HATEM S Z, WU Pei-dong. Crystal plasticity based modeling of grain boundary sliding in magnesium alloy AZ31B sheet [J]. Transactions of Nonferrous Metals Society of China, 2021, 31: 138−155.

线径压缩率对微细铜线材拉拔变形的影响

皇 涛[1]，吴捍疆[1]，宋克兴[1,2]，张彦敏[1]，周延军[1]，李韶林[1]

1. 河南科技大学 材料科学与工程学院，洛阳 471023；
2. 河南省科学院 材料研究所 河南省先进导体材料重点实验室，郑州 450000

摘 要：基于率相关晶体塑性理论，建立纯铜微细线材拉拔变形晶体塑性有限元模型，研究线径压缩率对线材拉拔过程中细观力学变形行为的影响。结果表明，经过拉拔的线材内部变形和滑移均呈不均匀分布状态，形成明显的滑移区和非滑移区，在拉拔线材内部产生了水平应变集中带。随着线径压缩率的增大，拉拔变形区线材内部的滑移系强度和滑移区域面积均逐渐增大。然而，线材拉拔变形区的接触压力和摩擦应力所引起的线材表面波动性受力状态使拉拔成形后的线材表面粗糙不平、拉拔过程平稳性降低。

关键词：微细铜线材；拉拔变形；晶体塑性；有限元；滑移机制

(Edited by Wei-ping CHEN)